Multiphase flow imaging through X-ray microtomography : Reconsideration of capillary end-effects and boundary conditions

Franck Nono[1,*], *Peter* Moonen[1,2], *Hélène* Berthet[3] and *Richard* Rivenq[3]

[1]CNRS/UNIV Pau & Pays Adour/E2S UPPA, Développement des Méthodologies Expérimentales-IPRA UMS3360, Pau, France
[2]CNRS/Total/UNIV Pau & Pays Adour/E2S UPPA, Laboratoire des fluides complexes et leurs réservoirs-IPRA UMR5150, Pau, France
[3]TOTAL S.A., Pau, France
[*]*now with Modis, Pau, France*

Abstract. We focus on capillary end-effects and boundary conditions during multiphase flow experiments. To that extent, we performed drainage and imbibition experiments on Bentheimer plugs with various wettabilities and for various flow rates. For each case, we studied the fluid distribution inside the pore space by means of X-ray microtomography. Experimental observations focus on three main aspects: (i) fluids distribution in the diffusers, (ii) saturation profiles and, (iii) cluster dynamics near the outlet-end interface.
It is shown that there is always an end-effect near the last cm/mm which cannot be investigated by many routine SCAL devices. Furthermore the outlet saturation varies significantly with flow rate, which disagrees the widely used zero capillary pressure (P_c) condition at the outlet corresponding to very little variation of the outlet-end saturation. In a standard configuration (inlet end piece – rock – outlet end piece) the observed filling states of the rock's interfaces contradict usual mathematical boundary conditions imposed on flow equations and the outlet end-piece may act (depending on geometry) as an obstacle to the flow direction thus generating perturbations and disturbing saturation profiles.
These experimental observations confirm the general conclusions that the physics of multiphase flow towards the boundaries in DRP and traditional SCAL experiments may be insufficiently known.

1 Introduction

Digital rock physics (DRP) has undergone remarkable developments these last years. Multiphase flow can directly be visualized at the pore scale under reservoir conditions and processes such as ganglion dynamics and snap-off can be investigated in great detail [1]-[3]. Nevertheless, the properties derived through DRP experiments still suffer from large uncertainties when compared to Special Core Analysis Laboratory (SCAL) data. Scarce studies [4], [5] succeeded in obtaining comparable experimental data via DRP routines as by classic SCAL measurements. One of the many reasons why there are large uncertainties associated to DRP routines is related to the sample size which is typically one or two orders of magnitude smaller than for SCAL. This raises questions about the representativeness of the results and more specifically the impact of experimental artefacts, mainly capillary end-effects (C.E.E) on the multiphase flow properties measured. On mm-scale plugs, these effects are expected to be emphasized. Analytical investigations [6], [7] have highlighted a clear relationship between the sample's length and the extent of C.E.E.
In this paper, we investigate C.E.E during classical oil-brine unsteady-state flow (USS) displacements at the pore-scale by means of 3D X-ray microtomography. Even though mathematical boundary conditions of a plug during USS flow displacement ((i) constant inlet injection rate, (ii) constant outlet pressure, (iii) zero Pc just outside the outlet face) and experimental considerations (total wetting of the inflow face by the injected phase) are widely used and mentally granted, there is little direct visual evidence to support these theories. This experimental study shows directly in a core flooding scenario and in agreement with a few conceptual and theoretical studies [8], [9] that our understanding of the boundary conditions during multiphase flow displacements may be less solid than that generally assumed. Before reporting our experimental results, we present a state of the art about end-effects. This concise literature survey includes a number of studies which report results that contrast with the general vision of boundary conditions. All along this paper, the discussion will be limited to USS flow displacements in homogeneous core samples.

2 State-of-the-art on capillary end-effects

C.E.E are essentially related to the boundary conditions of a plug during multiphase flow. At laboratory scale they arise due to the finite length of plugs and are most of the time significant whereas at the field scale they are negligible [10]. Capillary pressure being the difference in

* Corresponding author: franck.nono@external.total.com

the pressure in the non-wetting phase and that in the wetting phase, leads to be coupled with saturation inside the rock while this coupling does not exist outside the rock. A mathematical condition of Pc = 0 is then imposed at these boundaries (mainly outside the outlet end of the plug for USS flow) to solve flow equations.

Different causes for the saturation distortions at the inlet have been proposed. Nooruddin and Blunt [11] explained that some degree of counter-current flow of the non-wetting fluid is encountered across the inlet boundary during the injection of the wetting phase because the non-wetting phase may easily escape back through the inlet at the beginning of the test due to the capillary suction of the wetting phase by the rock, which impacts the saturation profile provided that water wetness is significant. Virnovsky et al. [12] argued based on numerical simulations that oil counter-current flow effects during waterflooding of a water-wet rock could be drastically reduced using a hydrophilic semi-permeable disk at the inlet. Other parameters such as (i) viscous fingering, (ii) plug's length and (iii) inlet end-piece geometry and properties are known to affect inlet end saturation. As the measured transient pressure drop over the overall plug length also depends on the inlet saturation, this artefact may cause non-negligible uncertainties on derived multiphase flow properties [13].

The most well-known capillary end-effects are related to the boundary conditions at the outlet-end. This subject has been extensively studied, especially in view of accounting for C.E.E during relative permeability (K_r) calculations using directly SCAL measurements or history matching of production and pressure data [12], [14]-[18]. A long-standing hypothesis in many SCAL studies is that the capillary pressure at the outlet-end (just outside the core's outflow face) equals zero, as it is assumed that the fluids exit the porous medium at equal pressure. This hypothesis has a number of logical consequences: (i) where both fluids are in contact at the outlet, the curvature must be negligible, (ii) the saturation being solely dependent on the capillary pressure, the outlet-end saturation must vary within very narrow limits thus be nearly independent on the flow rate, and (iii) at least the displaced phase must be continuous at the outlet-end. A small number of studies exist which report contradicting observations.

We start our introduction to this topic with the studies of Levine [19]. His set-up was one of the first attempts to measure the capillary pressure gradient over the plug's length during USS flow. A linear extrapolation of the measured P_c gradient to the outlet end seemed to indicate that the outlet P_c was not null at equilibrium. Later, Houpeurt [20] reported results of experiments performed by Delclaud for a private communication. Delclaud achieved vertical gas/oil drainage with gas (non-wetting phase) injected from the bottom of the sample and the outlet submersed in a large oil (wetting phase) volume. Under these conditions, he observed non-flat interfaces with gas bubbling out, indicative for non-null capillary pressure. Furthermore, he observed that an increase in gas pressure at the inlet generates an increase of the number of outlet pores occupied by gas. He argued that the outlet capillary pressure must at least be equal to the displacement pressure [21]. More recently, some authors [22] benchmarked various flow simulators including CYDAR ® [http://www.cydarex.fr] and the open source simulator SCORES [23]. They investigated the impact of different ways of imposing the outlet mathematical condition zero capillary pressure on the simulated production data and pressure gradient. SCORES is especially built in a way that it allows the outlet saturation to be flowrate dependent. Though, the outlet saturation variation range is too limited to observe an influence on production data or gradient pressure. It came out from this study that there were no impact on the different outputs.

From another perspective, when using conventional configurations of the outlet diffuser (i.e. an end-piece with grooves), mathematical boundary conditions may be very difficult to realise. Firstly, the end-piece acts as obstacle to the flow and generates perturbations as the flow stream lines near the interfaces are no longer straight [24]. Secondly, as pointed out by Ramakrishnan and Capiello [25], the outlet diffuser can unexpectedly become 100% saturated with one phase. For example, let us consider a stable vertical oil/brine primary drainage with oil injected from the top in a water-wet core. At equilibrium, a long time after breakthrough, there will be no brine in the diffuser and the rock's outlet-end will then be wetted by oil. Capillary pressure (P_c) at the outlet will therefore be impossible to characterize as there will be no interface. The semi-dynamic method [24] was implemented to correct this bias. With an optimized apparatus, the displaced phase is reinjected in the outlet diffuser through a different channel than that of normal flow at a very low rate so as to wash the core's outlet face and maintain its continuity from inside the plug to the diffuser, without disturbing the flow inside the core. The comparisons made by the authors with numerical simulations showed good agreements especially at low flowrates. However, at higher rates, the saturation gradient near the outlet end interface (where P_c is relatively small) does not match well. Unfortunately, we are not aware of any experimental verification of the actual saturation distribution in the immediate vicinity of the outlet-end for the semi-dynamic method.

Standard in-situ saturation monitoring (ISSM) does not always provide information enabling to verify the outlet P_c mathematical condition on the last cm of the sample and not at all on the last mm. The saturation profiles in these locations are always simulated, whereas the pressure gradient is measured along the rock's total length. If they exist, C.E.E in these last centimetres/millimetres may contribute significantly to the measured pressure gradient thus to the calculated relative permeability especially when using analytical approaches.

At this point, a parallel can be drawn with observations made regarding capillary pressure curves determined by the centrifuge method. The outlet boundary condition termed "zero capillary pressure" is the key assumption to derive P_c curves. For primary drainage curves, 100% of brine saturation is expected at the outlet. Some studies show that the zero capillary pressure assumption is not valid above a specific bond number or when using specific end-pieces [26]-[28]. They reveal a large number of issues and show that accurate criteria enabling a direct

experimental observation and quantification of these effects is lacking.

The difficulty in accessing the direct visualization of these phenomena is unlocked thanks to 3D X-ray microtomography. The drawback of using this technique is a matter of sample size. In practice, targeting higher resolution (tens of µm or less) imposes the use of millimetre-sized plugs and with small lengths (up to 10cm). Capillary end-effects are thus expected to be emphasized. Reducing C.E.E can be achieved by using long cores, high flowrates or high viscosity ratios. These choices are reflected in the Rapoport criterion (N_R) [29]:

$$N_R = L.v.\mu \geq 1 \text{ to } 5 \quad (in\ cm^2.min^{-1}.cP) \qquad (1)$$

Where L represents the sample length (cm), v the rate of displacement ($cm.min^{-1}$), and µ the displacing phase viscosity (cP). This factor is widely used in petrophysical applications mainly for the design phase when trying to set configurations reducing the impact of C.E.E. Many other factors can impact C.E.E such as permeability or rock-type. This is why even after Rapoport scaling, C.E.E may not be sufficiently minimised [18].

Recent studies [3] have evidenced different fluid flow configurations and cluster morphologies which are flowrate dependent (ganglion dynamics and connected pathway flow) and highlighted their important impact on K_r in some cases. The Rapoport criterion enables estimating that one would need to analyse samples in the order of at least one-half meter in length, to mimic in example waterflooding at reservoir rates (1ft/day) in the lab with negligible C.E.E. This sample size can't be used in conventional micro-CT devices. This example clearly illustrates that: i) We do not have a lot of flexibility, ii) We can't avoid to really understand C.E.E mechanisms and their impact on small cores, and iii) Depending on the rock/fluids/rates system, the entire rock length could be in the C.E.E.

The aim of the current study is to take a close look to what really happens near the sample boundaries in a conventional configuration (plug and diffusers) during oil and brine flooding at various wettability conditions and to understand the impact these phenomena may have on multiphase flow properties.

3 Materials and methods

The experimental set-up is similar to the one used by Berthet et al. [4].

3.1 Porous media

Flooding experiments were performed on eight cylindrical Bentheimer sandstone plugs (6 with diameter 4mm and 2 with diameter 1cm, lengths ranging from 1 to 5cm and modal pore size ranging from 60µm to 80µm). Bentheimer sandstone is widely used in the field of digital rock physics because only a small fraction of the pore volume is below the resolution of conventional X-ray micro-tomographs. Moreover, this rock-type is known to be homogeneous as illustrated by Figure 1 which represents porosity and permeability profiles along the full length of all eight plugs used in this study. Porosity was determined through 3D image processing. The porosity held in the clay fraction is below image resolution (4µm – 5µm) and is not taken into account. Differences between the calculated and the true porosity are estimated to be in the range of 1-2 porosity units (p.u.). Permeability was obtained using simulation on segmented images via OpenFoam ® software (Volume Of Fluid method implemented). Every permeability point is calculated over 500 µm length of the sample. Samples permeability varied between 1.3D and 2D with homogeneous profiles and an increase in the last 500µm due to trimming. With homogeneous profiles of permeability and porosity, the samples used in this study can be considered to be homogeneous.

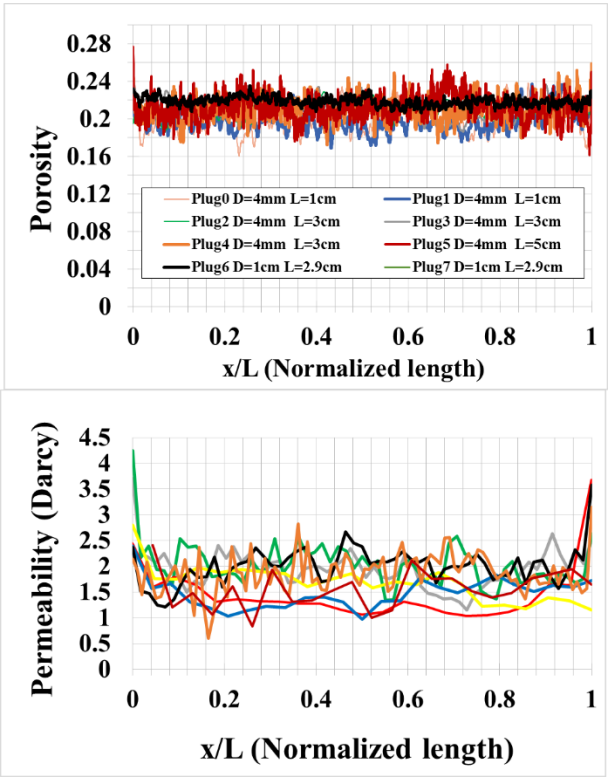

Fig. 1. Porosity and permeability profiles obtained via 3D image processing of the Bentheimer plugs used in this study and numerical simulation using segmented images on OpenFoam ® respectively. For porosity, the uncertainty on segmentation is estimated at +/- 0.4 p.u. and we must add +1 to 2 p.u. for the clay part.

3.2 Fluids

In this study, we focus on two phase flow (oil/brine) displacements. We use a brine made of 70 g/l of potassium iodide (KI) diluted into distilled water. This concentration enables sufficient X-ray contrast between oil, brine and rock. Decane was used as oil (μ_o = 0.93 cP and ρ_o = 0.73 $g.cc^{-1}$ at 25°C).

3.3 Wettability modification

Fresh Bentheimer sandstones are water-wet. For a certain number of tests (4), the natural rock wettability was altered after primary drainage following the protocol proposed by Tweheyo et al. [30]. The procedure consists in replacing the decane present in the plug by a mixture of decane and Hexadecylamine and letting the plug age for 24h at ambient temperature. The modified oil mixture is prepared by dissolving 8g/l of Hexadecylamine (acid additive) into decane for about two weeks. This period of time (2 weeks) is due to the fact that there was some excess amine which needed more time as it remained undissolved during the first days [30].

3.4 End-pieces (diffusers)

Two different geometries were manufactured in PEEK (Figure 2).

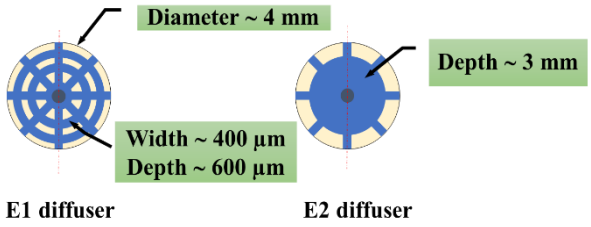

Fig. 2. Diffuser's geometry

i. The first diffuser (**E1**) features a pattern consisting of concentric circular grooves and straight radial grooves. The depth and width of the grooves are larger than the pore sizes in Bentheimer sandstone. Variants of this geometry are widely used in many laboratories worldwide.

ii. The second diffuser (**E2**) features a large central hole with a diameter nearly equal to the sample diameter and a depth (~3-5mm) much larger than the typical pore size of Bentheimer sandstone. This geometry causes minimal disturbance for the displaced fluid. Moreover, it allows live visualization of the fluids at the free-outlet interface of the plug during the experiment. Finally, as will be shown, **E2** end-pieces also help imposing mathematical boundary conditions at the outlet i.e. ensuring the continuity of the displaced phase and the permanent contact between the injected and the displaced phase at the oulet (see Delclaud experiments explained in the **State of art of capillary end effect** previously).

3.5 Image acquisition and processing

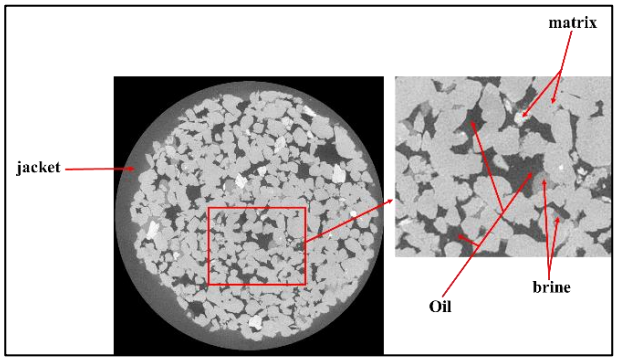

Fig. 3. Colour code for the reconstructed data

Figure 3 illustrates the colour code for reconstructed data ranging from dark grey for oil, light grey for the matrix. Intermediate grey levels correspond to brine.

Two different types of acquisitions were performed:

i. 3D scans of the whole plug after reaching steady-state conditions using end-pieces **E1**, and

ii. dynamic 2D and 3D scans of the plug's end faces during multiphase flow using end-pieces **E2**.

3D images were acquired using a Zeiss Xradia Versa 510. Energy settings were chosen between 80kV and 90kV while power varied between 7W and 8W. The voxel size was 4 µm for the 4 mm diameter plugs and 5 µm for the 1 cm diameter plugs. This meant we had to stitch 9 segments which would take 18 hours in total (2h per segment).

Image processing was realized using Avizo Fire 9.0 ® and the free software ImageJ. An illustration of the different stages of the image processing pipeline is presented in Figure 4. The raw images are already corrected automatically from beam hardening and ring artefacts in the upstream of the process by the software.

The 3D images of the wet plug were first registered to the dry images so as to be perfectly stackable. The matrix didn't change during the whole flooding protocols and it was verified during all registrations steps. The Viton® sleeve which had a specific greyscale level is isolated on the dry scan images using ImageJ and is used as mask for the entire dataset.

The main advantage is that the full cross section of the cylindrical sample can be analysed. The later stages involved filtering (non-local means filter), watershed segmentation and 3D labelling to dissociate and quantify the different phases/clusters at each flooding step.

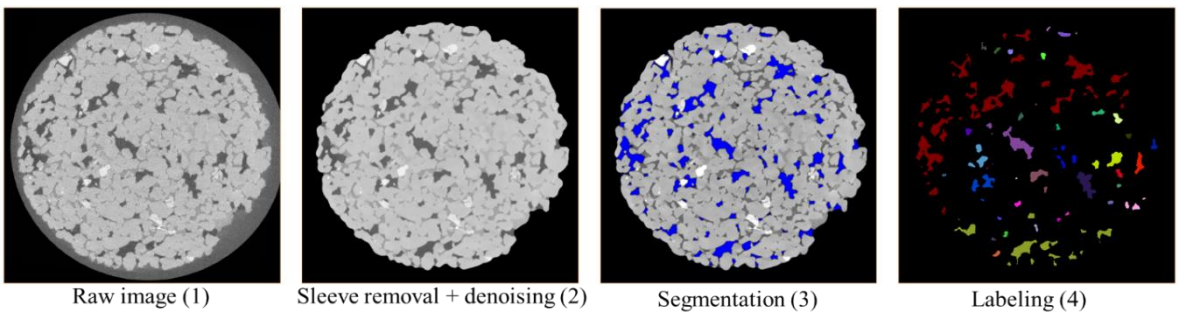

Fig. 4. Image processing of a Bentheimer sandstone

3.6 Experimental procedures

The following experimental procedure was used (end-pieces **E1**):

1. Dry 3D scan of the whole plug
2. Vacuum-saturation and flushing with 40 pore volumes (PVs) of brine
3. Vertical primary drainage with decane injected from top at different injection rates. At least 10PVs are injected at each rate. When steady-state conditions are reached, the flow is stopped and a 3D scan is taken under constant and stabilized pore pressure (15 bar). Dynamic scanning under steady state conditions was not possible due to limitations in capacity of the injection pumps.

N.B. Some tests were carried in the beginning of the project to evaluate the speed of redistribution of fluids in the core after stopping the flow during primary drainage steady-state. The conservation of saturation profiles was found to last more longer than the overall sample scanning time (18h).

4. Vertical waterflooding with brine injected from bottom at different injection rates. Similar to primary drainage, at least 10 PVs per step are injected and 3D scans are taken under stabilized pore pressure (15 bar).

Optionally, the wettability of the rock is altered in between steps 3 and 4. The flowrates used in this study are reported in terms of capillary number (C_a) expressed as below in equation 2:

$$C_a = v.\mu/\gamma \qquad (2)$$

Where v represents the superficial fluid velocity ($m.s^{-1}$), μ the displacing phase viscosity ($P_a.s$) and γ the interfacial tension ($N.m^{-1}$). The range of capillary numbers investigated is from $2.5x10^{-8}$ to $1.35\ x10^{-5}$.

4 Results and discussions

Results are divided into three topics:

i. Observations at the interfaces between the plugs and the **E1** end-pieces (inlet and outlet) at equilibrium
ii. Saturation profiles at steady state conditions (with **E1** end pieces)
iii. Experiments with **E2** end-pieces

All observations were well reproducible. The 8 samples followed almost the same procedure during primary drainage with similar qualitative observations. Saturation ranges (mostly the plateau of saturation profiles) varied within 5-6 units. Average saturations and saturation profiles during waterflooding for the 8 samples (4 in water-wet conditions and 4 in altered wettability conditions) varied within a narrower range (3 units max) than that for primary drainage with very similar qualitative observations.

However, in order not to overload the paper, each observation will only be illustrated for a single plug.

Regarding saturation profiles, they will always be illustrated with inlet at the left of the plot and outlet at right. Every point on saturation profiles represents an average over the diameter of the plug (4mm or 1cm) and a length which is the acquisition resolution (4μm or 5 μm).

4.1 Interfaces between plugs and E1 end-pieces

In Figure 5 we illustrate oil/brine distributions on 2D cross-sections during primary drainage at equilibrium for $C_a = 2.5x10^{-8}$ on strongly water-wet sample. The top left figure shows the inlet **E1** diffuser, and the other figures correspond to cross-sections at increasing distance from the inlet. The bottom right figure shows the outlet **E1** diffuser. The images show that the inlet and outlet diffusers are completely saturated with oil. This observation holds for different injection rates. Specifically concerning the presence of oil at the outlet, our observations confirm the expectations of Ramakrishnan and Capiello [25] and disagree the hypothesis that the outlet interface between the rock and the diffuser is almost 100% brine-filled. The cross-section with the highest brine saturation is located at almost 1 to 2 mm from the outlet diffuser, inside the plug and no connected brine flow path to the outlet could be identified.

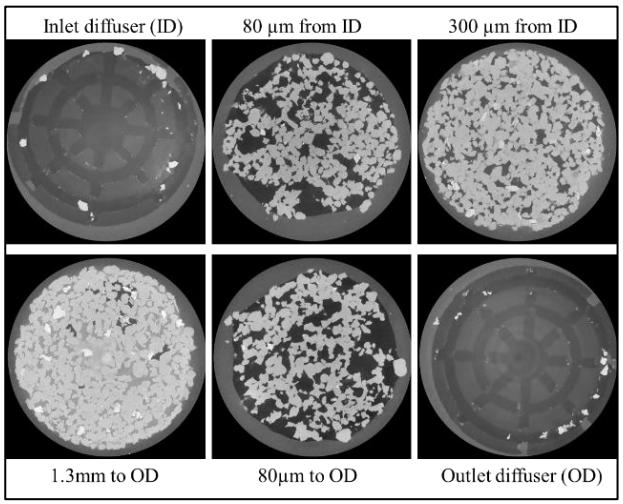

Fig. 5. From inlet (ID) to outlet (OD) during primary drainage of a 4mm diameter Bentheimer plug

Figure 6 uses a similar representation to illustrate the results after waterflooding. For the water-wet case (Figure 6a) the inlet is full of oil trapped in the diffuser due to (i) counter-current flow and (ii) the presence of large pores near the end-faces, leading to oil trapping in the first 100μm of the plug. Oil and brine co-exist inside the plug, oil occupying the large pores and brine the smaller ones as expected for this wettability. Near the outlet, a large fraction of the diffuser is oil filled while at 80μm from the outlet surface, brine fills the majority of pores. The filling in the diffuser could be for the most relevant due to the imperfect contact between the plug and the end-piece (trimming) or rock's wettability. As will be shown in Figure 6b, diffuser's wettability seems to have a negligible impact on fluid's repartition.

For the altered wettability case (Figure 6b), the inlet diffuser is full of brine (as expected) contrary to the water-wet case. Inside the sample, brine occupies the larger pores, while oil is found in the smaller ones. Close to the outlet of the plug we observe an accumulation of oil as expected due to the capillary end effect. The diffuser is however full of brine.

These reproducible observations per rock's wettability show that the inlet diffuser, as well as the space between the inlet diffuser and the sample, is not necessarily filled with the injected phase. On the contrary, rock's wettability seems to be the determining factor. When comparing tests at different flow rates (not shown) for the takes place from left to right (representing the sample top and bottom respectively).

All profiles exhibit a brine saturation increase towards the end of the plug, which is the typical signature of C.E.E. As expected, C.E.E. decreases with increasing injection rate. We observe 100% oil saturation at the injection face.

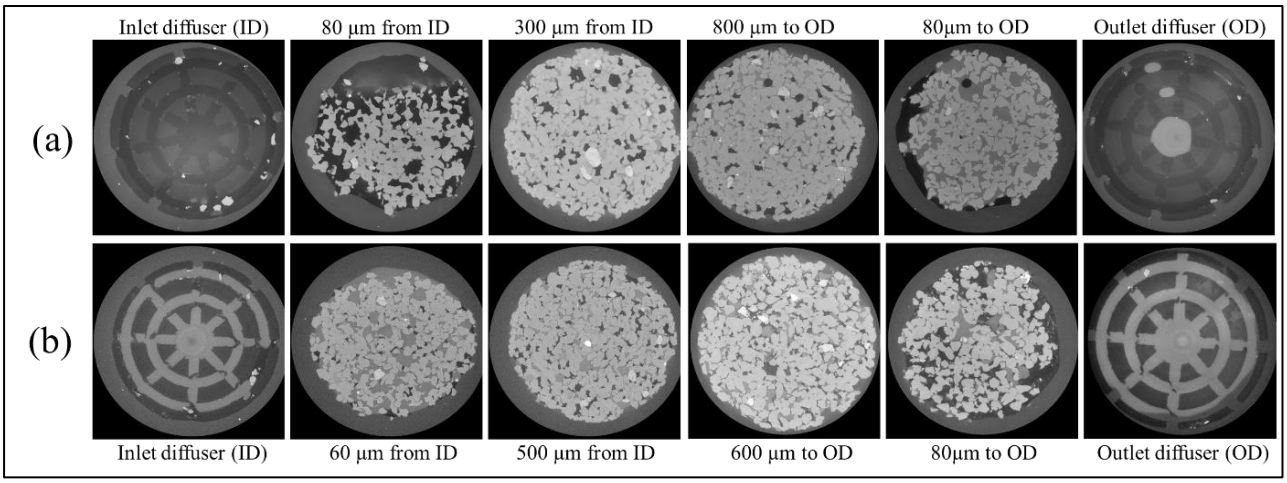

Fig. 6. From inlet to outlet during waterflooding of Bentheimer: (a) water-wet case at Ca=1.35x10^{-7} ; (b) altered wettability case at C_a=1.35x10^{-7}

waterflooding in the water-wet case, we observe that once a preferential flow path is formed through the whole plug at low flow rate, it becomes very difficult to evacuate the trapped oil phase at the inlet even when we increase the flow rate within 2 orders of magnitude. A full contact between the injected phase and the entire area of the plug's inlet face may thus be difficult to obtain and control during unsteady-state flow experiments depending on rock's wettability.

Important observations are also made near the outlet end. At this interface just inside the plug, saturation is expected to tend to the corresponding zero capillary pressure saturation and just outside the plug, a permanent contact between both fluid phases is expected. Our observations show that this is not necessarily true as for example in the primary drainage case, the outlet volume is 100% filled with oil and oil wets the entire outlet face of the plug. These observations hold regardless of the rock wettability, the diameter-to-length ratio of the sample and the investigated flowrate. Repeatability tests were performed as well. All these results seem to indicate that mathematical boundary conditions are not necessarily satisfied during drainage and imbibition experiments on micro-plugs in this particular configuration.

4.2 Saturation profiles

4.2.1 Primary drainage of water-wet samples

Figure 7 and Figure 8, illustrate primary drainage saturation profiles at different oil injection rates (characterised by the capillary number) for two water-wet samples of respectively 4 mm and 1 cm in diameter. Both samples have a length of 29 mm. Each saturation profile curve is obtained after the injection of a sufficient number of pore volumes to ensure dynamic equilibrium. The flow

Few grains after the injection face just inside the core plug, saturation values exhibit an apparent plateau which level depends on the injection rate. This observation shows that the plug is entirely in C.E.E which then could invalidate an analytical approach [18] of determining relative permeability. It is similar from what reported in [18] for their case0 (also entirely in C.E.E). Very close to the outlet face of the plug, all brine saturation profiles exhibit a steep drop. This observation is coherent with the displacement of all the brine by oil in the outlet diffuser as shown on Figure 5. Note these saturation gradients occur over a very short distance, less than 10 mm, which is too small to be detectable by some routine SCAL devices and could erroneously be interpreted as a plateau without capillary end effects.

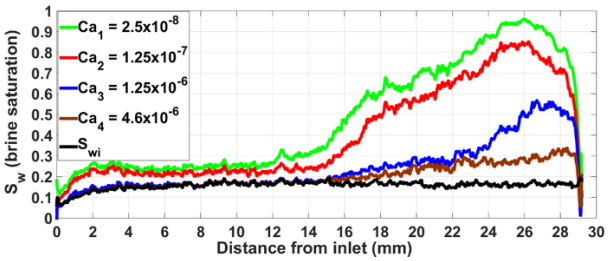

Fig. 7. Example of brine saturation profiles during primary drainage at varying injection rates of a Bentheimer plug (sample diameter = 1cm)

C.E.E in these zones could engender additional pressure gradient which may not be negligible for an interpretation using analytical methods. A final observation is that all saturation curves exhibit dependency on the injection rate: both the saturation level of the plateau in the first part of the plug (as expected) and the peak of maximum brine saturation in the second part of the plug are both capillary number dependent.

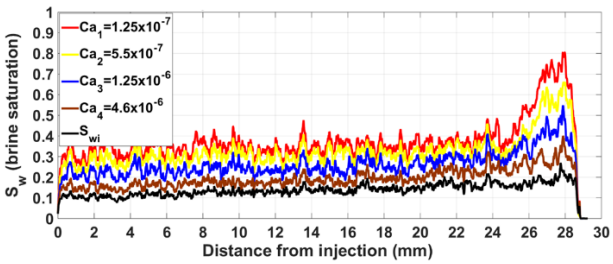

Fig. 8. Example of brine saturation profiles during primary drainage at varying injection rates of a Bentheimer plug (sample diameter = 4mm)

This second point contradicts the assumption that the peak saturation (point of maximum wetting phase saturation → outlet saturation in SCAL experiments) is independent of the injection rate (outlet P_c~ 0 → outlet S_w~ constant) during primary drainage [24].

At this stage, the most plausible cause for the difference between our observations and the expected saturation profiles seems to be that our boundary conditions differ from the mathematical ones. One can argue that the final average brine saturations obtained in our study during primary drainage with the flooding method (in the range of 10% to 15%) are greater than what obtained Lin et al. [31] on similar sample (7% - 10%) with centrifugation method meaning that we still have a mobile brine saturation on the last drainage rate. Initialization by flooding is known to not be an efficient method for SCAL protocols but here, it doesn't have an impact on our interpretations as the main points highlighted here occur before we reach our apparent irreducible brine saturation. We first seek to understand the dependency of the peak saturation with the injection rate. To that extent, the last few mm of the plug are analysed in detail. Figure 9 is a 3D representation of the (percolating) oil phase near the plug outlet. We clearly observe a very high oil content at the outlet next to the diffuser, corresponding to zero brine saturation and consistent with the observations made on figure 5. Slightly inward, we observe less oil, corresponding to the peak in water saturation. At increasing injection rates (i.e. capillary number), we observe the development of oil counter-current flow, leading to a local decrease in brine saturation. This was observed for all plugs investigated.

We assume that this phenomenon may be caused by perturbations at the outlet-end due to the diffuser. Lombard [24] argued that the distance affected by this perturbation could be estimated as the distance between the grooves of the diffuser. Our experiments seem to indicate that the counter-current flow can impact the saturation profiles at much larger distances from the outlet. When the capillary number is increased, the counter-current oil fingers grow and reconnect with the large percolating oil cluster in the bulk of the sample. Rather than only being controlled by the inter-groove distance, the phenomenon also seems to be pressure controlled. Our tests with an alternative diffuser, reported in section **4.3** seem to confirm this hypothesis.

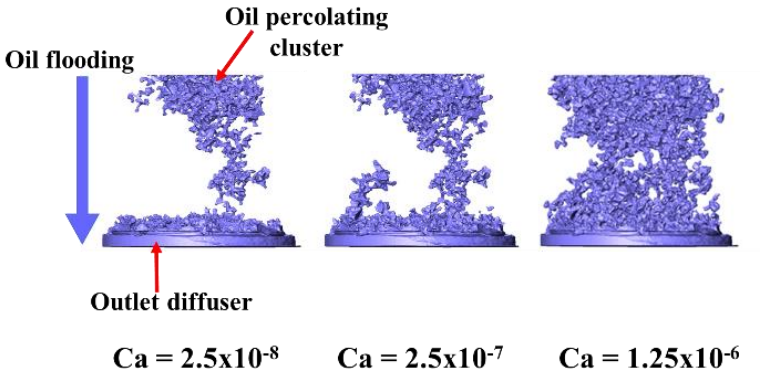

Fig. 9. Oil cluster spreading out and accumulating at the outlet during primary drainage of a Bentheimer plug (diameter = 4mm) at various rates. Magnification is the same in both directions and the diffuser is 4 mm diameter.

4.2.2 Waterflooding of water-wet samples

Figure 10 depicts brine saturation profiles of a 1cm diameter plug for various brine injection rates. These profiles are well reproducible, both qualitatively and quantitatively. As expected for water-wet plugs, the saturation is rather constant along the plug length and the flowrate does not have any impact on the measured residual oil saturation for the considered range. The average residual oil concentration S_{orw} lies between 40% and 45% for all the plugs investigated, and this range is consistent with literature data on Bentheimer sandstone [32]. As it was the case for primary drainage, we also observed distortions of saturation profiles near both end faces during waterflooding. The distortions at the inlet are consistent with counter-current flow and the presence of large pores near the inlet surface (Figure 6a) and thus we expected low brine saturation at low rates. At high injection rates, the oil cluster at the inlet is fractioned and transported downstream. Towards the outlet we surprisingly observe a reproducible brine saturation gradient (brine saturation increases along the plug). A detailed analysis of oil clusters over the plugs' length (see Figure 11) revealed that a large number of small clusters are trapped in the last 4-5 mm of the plug. This phenomenon is not yet explained.

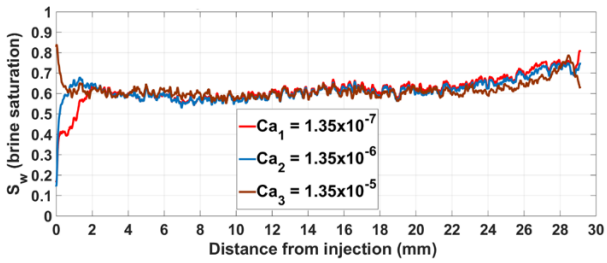

Fig. 10. Waterflooding of a Bentheimer sandstone operated at water-wet conditions : diameter = 1cm, length = 2.9cm

Among the possible causes, we cite: i) perturbations of the end-piece causing multidirectional flow near the last millimetres or ii) re-imbibition of brine after breakthrough. A simulation work is required to fully understand this phenomenon.

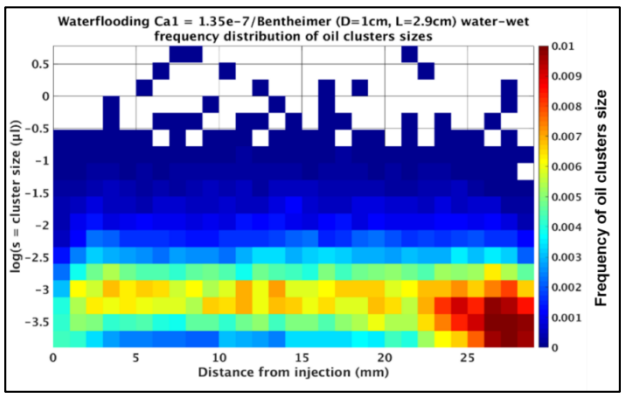

Fig. 11. Distribution of oil clusters size over the plug's length. Clusters smaller than 1000 voxels are not considered as they might be related to imaging artefacts. Every cluster is positioned according its center of mass

4.2.3 Waterflooding of altered-wet samples

The results of waterflooding experiments on a sample of Bentheimer with altered wettability are presented in Figure 12. As for the case of waterflooding on water-wet rocks, we observe a rather constant brine saturation level along the plug length which seems to be quite invariant with flowrate. The average remaining oil saturation (ROS) is lower than for the water-wet case (between 20% and 32% for all the plugs investigated and for all capillary numbers). These results are reproducible among all plugs investigated.

Close to the plug outlet-end, a peak in oil saturation (or a decrease in brine saturation) is observed. This end-effect moves towards the outlet end face as capillary number increases. Note that the average oil saturation decreases as rate increases. As the saturation gradient is concentrated over the last 3 mm, it would not be captured by conventional 1D ISSM (In Situ Saturation Monitoring). Our observation might explain the puzzling results of Heaviside [33] on macro cores: he reported decrease in average oil saturation with rate on intermediate wet samples without any saturation gradient. We can see here an analogy in observations with the primary drainage phase of the water-wet case. At both end

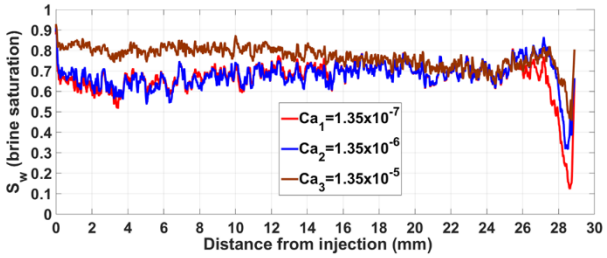

Fig. 12. Example of brine saturation profiles during waterflooding of a Bentheimer sandstone operated at modified wettability conditions, diameter = 4mm , Length = 2.9cm

surfaces of the plug, a high brine saturation is found, which is consistent with the saturation state of the diffusers (Figure 6b).

These observations on brine saturation profiles clearly show that our end-pieces have a significant impact on the distribution of the fluids in place. The resulting profiles do not match with the conventional theory of zero capillary pressure at the outlet face hence raising future, undeniable and quantitative investigations on the real impact of this phenomenon on relative permeability (K_r) or capillary pressure (P_c) curves determination in similar conditions.

4.3 Experiments with E2 end-pieces

To confirm the important impact of the end-pieces, we performed a series of drainage and imbibition tests with an alternative exit diffuser design. Furthermore, the microfluidics system was adapted to generate continuous flow during X-ray monitoring. Dynamic 2D radiographic imaging was performed as well as 3D imaging of the steady-state equilibrium configuration. Steady-state was assumed to be reached as soon as the pressure gradient remained constant over a time scale we fixed at 30 min.

In view of minimizing perturbations of the flow (and thus to impose near-ideal outlet flow conditions), **E2** outlet-end pieces feature a large free space and minimize contact with the sample. Secondly, the flow direction is reversed with respect to the conventional direction. This means that during primary drainage, oil is injected from bottom to top so as to maintain a large brine filled outlet on top of the sample over which the exiting oil floats. For waterflooding experiments, we altered rock wettability first and injected the brine from top to bottom so as to maintain contact between oil and the sample's outlet end by capillary affinity, while the exiting water sinks due to gravity.

Experiments were performed on two samples of 1 cm in diameter and 3 cm in length. This size is an intermediate length between plugs typically used in micro-CT experiments and those used in SCAL experiments. We first performed primary drainage and focussed on the outlet with 3D dynamic scans for three different steady-state flow rates without stopping oil flooding. Figure 13 shows a number of cross sections near the outlet surface of the plug for three different injection rates.

It is clear that the brine saturation increases towards the end of the plug. The outlet surface is nearly 100% brine

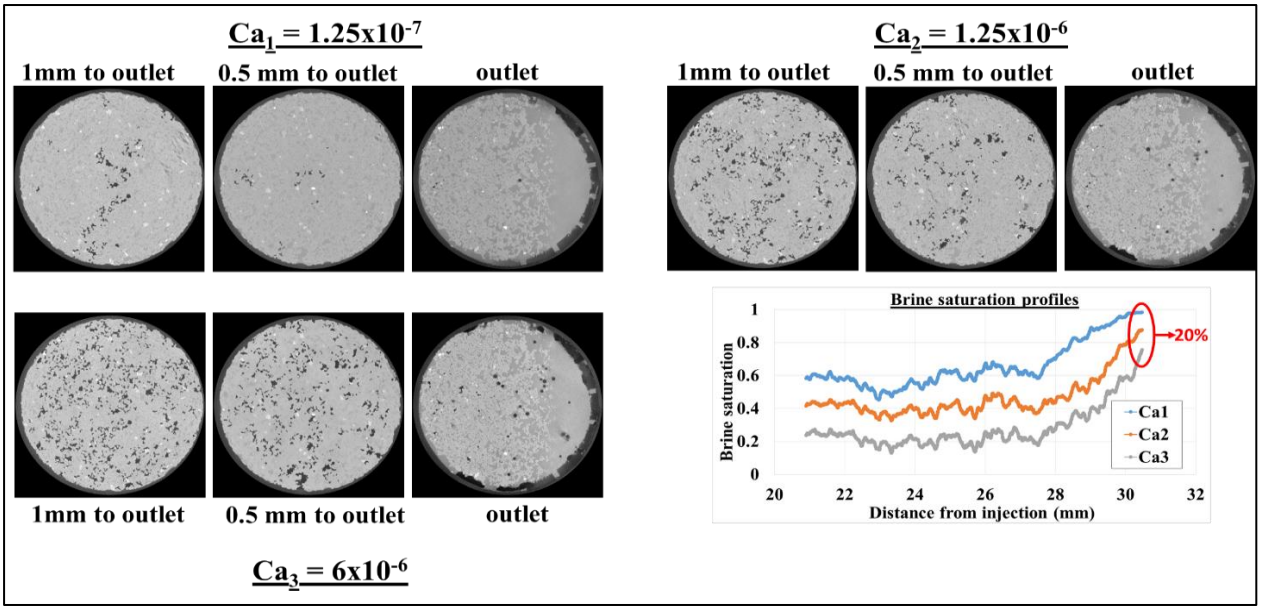

Fig. 13. 2D slices (from 3D reconstructed images) of the outlet-end interface with **E2** end-pieces during ascending primary drainage of a water-wet Bentheimer sandstone after reaching steady-state conditions for different injection rates. Saturation profiles are incorporated. One can see that the profiles follow a practically monotonic trend and a change of up to 20% of brine saturation is encountered at the outlet between the lowest and the highest capillary numbers investigated in this experiment. Though the range of capillary numbers investigated in this experiment is small so we expect more variations of the outlet saturation with greater ranges of capillary numbers.

saturated at the lowest rate. The maximum saturation is found at the exit plane, as expected. Here, brine is in permanent contact with the sample. The **E2** end pieces thus enable enforcing the expected boundary conditions (maximum water saturation at the outlet), and the resulting saturation profiles are much closer to the theoretical expected profiles. However, the decrease of the outlet brine saturation with increasing oil flowrate, disagrees with the theory of nearly constant outlet saturation. It would be interesting to check whether this inconsistency is also present in the semi-dynamic method. For the second test, a plug was drained with decane until irreducible brine saturation. After 2 days of ageing with modified decane [sufficient to alter wettability, see [30]], waterflooding was performed from top to bottom. 2D projections of the outlet were continuously acquired (at 1 Hz) after reaching steady-state conditions without stopping the flow. Characteristic projection images for three injection rates are shown in Figure 14.

As expected, at low Capillary number oil wets the majority of the plug's outlet surface. At a number of discrete locations, brine droplets exit the sample. Once they reach a critical size, these droplets detach and sink. When the brine flowrate is increased, we observe an increase in the number of brine exit points. This implies that the brine saturation at the outlet plane increases with increasing flowrate. This result is similar to the observations reported by Houpeurt [20] in the gas-oil

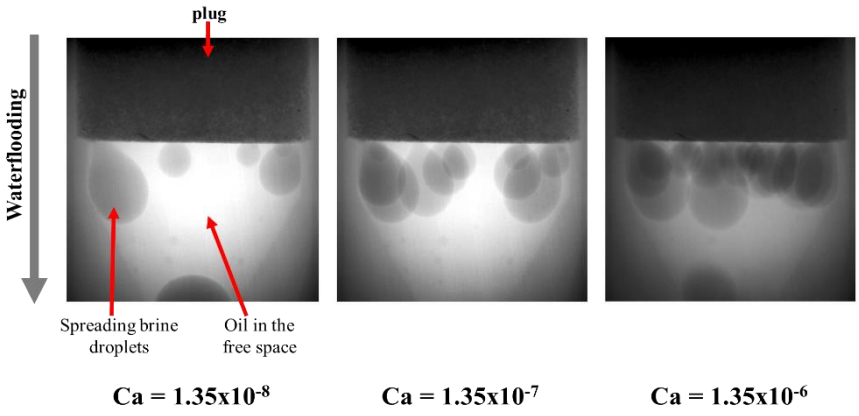

Fig. 14. 2D projections of the outlet-end interface with **E2** end-pieces during waterflooding of Bentheimer sandstone after reaching steady-state conditions for different injection rates. The wettability in this case is modified using the mixture of decane and hexadecylamine at S_{wi}. Brine is dark grey and oil is light grey in opposite to 2D tomograms (e.g. Fig.2.) where brine is light grey and oil is black.

system during gas injection. Furthermore, in this dynamic configuration, the interface curvature of each droplet is constantly changing. One can measure the droplets curvatures to: (i) determine the true outlet boundary condition, (ii) relate the capillary pressure calculated to a Pc–S_w curve. In primary drainage mode with oil injected from bottom to top and a free outlet full of brine, oil droplets were very difficult to capture due to their small sizes and rapid motion thus impossible to measure a curvature. We did measure manually brine droplets curvatures for wettability conditions depicted in figure 14 (altered wettability state) as the motion was slower and brine droplets were bigger. Unfortunately, we didn't achieve measurements of capillary pressure curve at this wettability.

In real time, the brine droplets are in a dynamic motion, increasing their volume then breaking and falling down the diffuser due to gravity forces. Though for measurements, we assumed them to be static and axi-symmetrical. The highest capillary pressure measured was found when the droplets just appeared at the interface. Values of almost 4 to 5 mbars of capillary pressure were measured. When the droplets grow, the curvatures become wider and Pc decreases to negligible values (0.2 mbars) before collapse. They all (brine droplets) had similar curvature values even when their number increased. One reason could lie on the fact that the zero capillary pressure zone on the Pc curve may be very flat and a little variation of capillary pressure could head to a great variation of brine saturation at the outlet.

4.4 Attempt to Darcy-scale simulation of experimental saturation profiles

In other to investigate the possible impact of misunderstanding capillary end effect behaviour on the determination of multiphase flow properties, we first tried to understand if our saturation profiles obtained during primary drainage (case with most available data in the literature) could be simulated with a Darcy scale approach. The main idea here is to simulate saturation profiles during primary drainage using literature data (primary drainage Pc– S_w curves and relative permeability curves of Bentheimer sandstone can be found in [31] and [34] respectively) and compare them to our experimental profiles. For indication, we used: irreducible brine saturation of S_{wi} = 7%, Corey fit exponents of n_w = 4.1, n_o = 3.2 and end-point K_{row} of 0.98. The softwares **CYDAR ®** and **SCORES** were used to simulate saturation profiles and both simulators outputs were also compared. However some considerations needed first to be taken into account. As the sharp decrease of brine saturation near the outlet during primary drainage can't be simulated at the Darcy-scale, the last 2mm of the sample are truncated (beginning at the peak of brine saturation, see Figure 15 which are saturation profiles from Figure 8). The choice of saturation profile on the last 2mm is then let free to the simulators. The first comparisons between simulation and experiments didn't work that well because the capillary pressure used was found to be high.

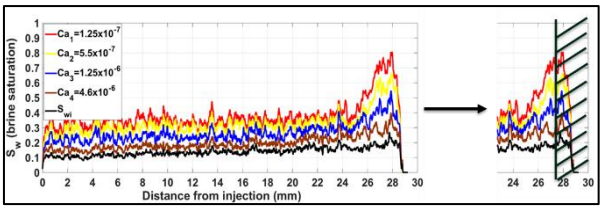

Fig. 15. Preparing experimental saturation profiles for history matching

History matching of experimental saturation profiles shown that the best capillary pressure curve explaining our data was almost half in values than that of Lin et al. [31]. This may be due to differences in IFT values used. The authors reported an IFT of 51.5 mN/m in their experiments. In our study, we used n-decane and unfortunately, we couldn't measure the true brine/decane IFT. The expected value is nearly 35 mN/m.

Comparisons of simulated saturation profiles and experimental data are reported in figure 16 in the top figure. The experimental data is well matched (apart from the lowest capillary number) and both simulators gave similar results although different implementations of mathematical boundary conditions as expected in [22].

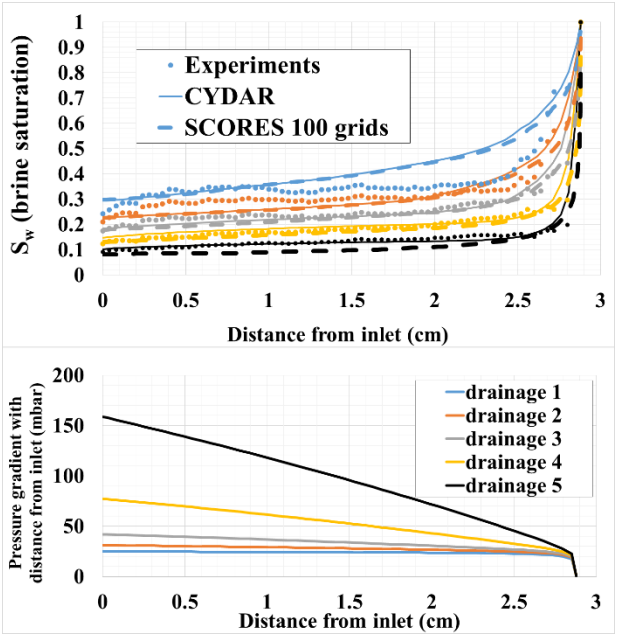

Fig. 16. top figure - comparisons of simulated saturation profiles (results from CYDAR and SCORES) with experimental data; bottom figure - pressure gradient function of the position in the plug.

However, when we look at the gradient pressure profiles determined using CYDAR ® (figure 16, bottom figure), we can notice that at lower rates, the last millimeters of the plug gather an important part of the total gradient pressure. When the injection rate increases, this zone has less and less impact but still, at the highest capillary number, the last 2mm gradient pressure represents almost 10% of the total gradient pressure. Though, this is a simulated gradient pressure related to the simulated saturation profile. In reality, during experiments we observe a sharp decrease of brine saturation and not an

increase towards 100% S_w. We then expect the simulated gradient pressure in these last millimeters to be different from the experimental measurements, but to what extent ? This can only be answered through additional experiments and some pore-scale numerical simulations.

5 Conclusions

This paper presents a detailed analysis of capillary end effects during unsteady-state flow. The study relies on 3D X-ray microtomography and uses a microfluidic setup. We focus on multiphase flow in homogeneous Bentheimer sandstones and the observations were reproducible on all eight plugs investigated.
The main conclusions of this study are:

- Capillary-end effects always exist in the last centimeters or millimeters of the plug, i.e. at locations which might be invisible to some usual SCAL devices. The presence of Capillary end effects is systematic and may have an impact on the measured pressure difference over the plug.
- Outlet end saturation varies with flow rate. The theoretical concept of a zero capillary pressure boundary condition may be questionable. At low rates (nearer to field rate), this assumption can be applied without causing much errors. At higher rates, saturation distortion may have to be taken into account. The question remains to what extent they impact multiphase flow properties derived through interpretation by simulation;
- With the end-faces configuration used in this study, the expected boundary conditions were not guaranteed. Diffuser geometry and rock wettability are shown to have a critical impact on the obtained saturation profiles, and thus should be taken into account when interpreting multiphase flow experiments.
- Outlet end-pieces act as obstacles to the flow even though their geometry was intended to avoid that and it doesn't seem to be a matter of diffuser's wettability. They generate counter-current flow of the injected phase and thus drastically affect saturation profiles close to the outlet, which complicates history matching. Without an optimized apparatus, the best way to maintain theoretical wetting conditions and to avoid counter-current flow is adapt the diffuser geometry. The results obtained with our free outlet diffuser (**E2**) showed that saturation profiles are monotonic till the end faces.
- A Darcy-scale simulation of our experimental data shows that our saturation profiles are nearly in line with what is expected from the literature but the distortion of the profiles in the last millimetres occurs in a zone which could gather depending on rate, an important amount of the gradient pressure. It becomes therefore important to clarify the real impact of this **systematic** distortion on the experimentally measured gradient pressure as it could also have an impact on interpretation by simulation. Beyond a perspective of investigating the real impact of these observations on SCAL studies, one must keep in mind that a future best description of these systems should incorporate pore scale modelling in plugs AND in the whole outlet taking into account their geometry.

We thank TOTAL for their financial support and the permission to publish this paper. We also acknowledge Dr. G. Hamon, Dr. C. Caubit, Dr. Clement Varloteaux, Mme M. Hebert and Mr R. Brugidou for their insightful discussions and contributions.

References

1. M.G. Andrew, H. Menke, M.J. Blunt, and B. Bijeljic, "The imaging of dynamic multiphase fluid flow using synchrotron-based x-ray microtomography at reservoir conditions," in *Transport in porous media*, 110(1), 1-24, (2015)
2. S. Berg, H. Ott, S. A. Klapp, A. Schwing, R. Neiteler, N. Brussee, A. Makurat, L. Leu, F. Enzmann, J. O. Schwarz, M. Kersten, S. Irvine, and M. Stampanoni, "Real-time 3D imaging of Haines jumps in porous media flow," *Proceedings of the National Academy of Sciences*, 110(10), 3755–3759, (2013)
3. M. Rücker, S. Berg, R. T. Armstrong, A. Georgiadis, H. Ott, A. Schwing, R. Neiteler, N. Brussee, A. Makurat, L. Leu, M. Wolf, F. Khan, F. Enzmann, and M. Kersten, "From connected pathway flow to ganglion dynamics," *Geophysical Research Letters*, **42**(10), 3888–3894, (2015)
4. H. Berthet, P. Andriamananjaona, S. Barbouteau, M. Hebert, R. Farwati, R. Meftah, G. Quenault, J.P. Chaulet, , R. Brugidou, and R. Rivenq, "Capillary desaturation curves and insights on trapped oil at the pore-scale, in water-wet and oil-wet sandstones," *International Symposium of the Society of Core Analysts*, SCA2018 Trondheim, Norway, (2018)
5. S. Zou, F. Hussain, J. Arns, Z. Guo, and C. Arns, "Computation of relative permeability from in situ imaged fluid distributions at the pore scale*," SPE Journal*, n°189453, (2018)
6. D.D. Huang, and M.M. Honarpour, "Capillary End Effects in Coreflood Calculations," Paper SCA 9634 presented at the International Symposium of the Society of Core Analysts, Montpellier, France, 8-10 September, 1996.
7. R.Gupta, and D. R. Maloney, "Intercept Method - A Novel Technique to Correct Steady-State Relative Permeability Data for Capillary End-Effects," Society of Petroleum Engineers, (November 10, 2014), doi:10.2118/171797-MS.
8. E. Unsal, G. Mason, N.R. Morrow, D.W. Ruth, "Bubble snap-off and capillary-back pressure during counter-current spontaneous imbibition into model pores," Langmuir 25(6):3387–3395, 2009.
9. E. Unsal, "Impact of Wetting Film Flow in Pore Scale Displacement," SCA 2013–016 (2013)

10. R. Gupta, P. Lu, and R. Glotzbach, "A Novel Field-Representative Enhanced Oil Recovery Coreflood method," Improved oil recovery Symposium, Tulsa, 12-16 April. *Society of Petroleum Engineers*, http://dx.doi.org/10.2118/169088-MS (2014)
11. H.A. Nooruddin, , and M.J. Blunt, "Analytical and numerical investigations of spontaneous imbibition in porous media", *water Resour. Res.*, 52, 7284–7310, http://dx.doi.org/10.1002/2015WR018451, (2016)
12. G.A. Virnovsky, Y. Guo, S.M. Skjaeveland, and P. Ingsoy, "Steady-State Relative Permeability Measurements and Interpretation with Account for Capillary Effects," *Society of Core Analysts,* SCA1995-02, (1995)
13. C. Shen and D.W. Ruth, "Impact of inlet boundary conditions on the numerical simulation of one-dimensional coreflooding," *J. Can. Pte. Technol.,* **35**, 1, pp. 19-24, (1966)
14. R. Gupta and D. R. Maloney, "Intercept method-A novel technique to correct steady-state relative permeability data for capillary end effects," *Society of Petroleum Engineers*, http://dx.doi.org/10.2118/171797-PA, (2016)
15. G. F. Hadley, and L. L. Handy, "A theoretical and experimental study of the steady state capillary end effect," *Society of Petroleum Engineers*, http://dx.doi.org/10.2118/707-G, (1956)
16. S. Qadeer, K. Dehghani, D.O. Ogbe, and R.D. Ostermann, "Correcting Oil/Water Relative Displacement Experiments," *Society of Petroleum Engineers,* SPE 17423, presented at the SPE California Regional Meeting held in Long Beach, March 23-25, (1988)
17. R. Gupta, and D. Maloney, "Applications of the Intercept Method to Correct Steady State Relative Permeability for Capillary End Effects," Paper SCA2015-001 presented at the SCA International Symposium, St. John's Newfoundland and Labrador Canada, 16–21 August, 2015.
18. J. Reed, and J. Maas, "Review of the intercept method for relative permeability correction using a variety of case study data," In The International Symposium of the Society of Core Analysts, Trondheim, Norway , 2018.
19. J.S. Levine, "Displacement experiments in a consolidated porous system," *Trans. AIME* **201**, 57, (1954)
20. A. Houpeurt, « Mécanique des fluides dans les milieux poreux - Critiques et recherches, » Editions Technip, Paris, (1974)
21. J. P. Delclaud, "New results on the displacement of a fluid by another in a porous medium," http://dx.doi.org/10.2118/4103-MS, *Society of petroleum engineer*, (1972)
22. R. Lenormand, K. Lorentzen, J.G. Maas, and D. Ruth, "Comparison of four numerical simulators for SCAL experiments," International Symposium of the Society of Core Analysts (August 2016), Snowmass, USA, SCA-2016-006, 2016.
23. J.G. Maas, and A.M. Schulte, "Computer Simulation of Special Core Analysis (SCAL) Flow Experiments Shared on the Internet," Reviewed Proceedings of the 1997 International Symposium of the SCA, Calgary, Canada, September 7-10, 1997.
24. J.M. Lombard, P. Egermann, and R. Lenormand, "Measurement of capillary pressure curves at reservoir conditions," SCA n° 2002-09, *Society of Core Analysts*, Monterey, California, (2002)
25. T. S. Ramakrishnan, and A. Cappiello, "A new technique to measure static and dynamic properties of a partially saturated porous medium," *Chem. Eng. sci.* **46**, 1157−1163, (1991)
26. D.J.Jr. O'Meara, G.J. Hirasaki, and J.A. Rohan, "Centrifuge Measurements of Capillary Pressure: Part 1-Outflow boundary condition," *SPE Res Eng* 7(1): 133-142, SPE-18296-PA, http://dx.doi.org/10.211 8/18296-PA, (1992)
27. D. Ruth and Z. Chen, "On the measurement and interpretation of centrifuge capillary pressure curves: The SCA survey data," *The log Analyst*, 36, 21, (1995)
28. R. W. Wunderlich, "Imaging of Wetting and Non-Wetting Phase Distributions- Application to Centrifuge Capillary Pressure Measurements," 60th Annual Technical Conference and Exhibition, September 22-25, Las Vegas, Nevada, *Society of Petroleum Engineers,* SPE Paper 14422, (1985)
29. L. A. Rapoport, and W. J. Leas, "Properties of linear waterfloods," *Trans AIME* **198**, 139-148, (1953)
30. M.T. Tweheyo, T. Holt, and O. Torsaeter, "An experimental study of the relationship between wettabilty and oil production characteristics," *J. Pet.Sci. Eng.* **24** (2-4): 179-188, http://dx.doi.org/10.1016/S0920-4105(99)00041-8, (1999)
31. Q. Lin, B. Bijeljic, , S. Berg, R. Pini, M. J. Blunt, and S. Krevor, "Minimal surfaces in porous media: pore-scale imaging of multiphase flow in an altered-wettability Bentheimer sandstone," https://doi.org/10.1103/PhysRevE.99.063105, 2019, March 28.
32. X. Nie, Y. Mu, R. Sungkorn, V. Gundepalli and J. Toelke, "Numerical Investigation of the Dependence of Residual Oil Saturation on Geometry, Wettability, Initial Oil Saturation and Porosity," Proceedings of the International Symposium of the Society of Core Analysts, SCA2014-042, Avignon, France.
33. J. Heaviside, C.E. Brown and I.J.A. Gamble, "Relative permeability for intermediate wettability reservoirs," paper SPE 16968 presented at the 62th Annual technical Conference and Exhibition of SPE, Dallas, TX, Sep. 27-30, (1987)
34. M. Blunt, "Multiphase Flow in Permeable Media: A Pore-Scale Perspective," Cambridge University Press. doi: 10.1017/9781316145098, 2017.